STRUCTURAL AND OPTICAL PATHLENGTH CONTROL EXPERIMENTS ON A PRECISION TRUSS

Zahidul H. Rahman*, John T. Spanos† and John O'Brien*‡
Jet Propulsion Laboratory
California Institute of Technology
Pasadena, California 91109

1, Abstract

An experimental implementation of a nanometer level optical pathlength controller for long baseline space interferometry is presented. The pathlength compensation system is tested on a large precision truss structure and thus structural dynamics play a dominant role in the control system design. The associated control structure interaction (CSI) problem and an impedance matching technique to enhance structural damping are elaborated. With a multi-layer approach consisting of structural control for damping augmentation and optical control for direct pathlength compensation, the optical pathlength variation is maintained within 6 nanometers RMS under laboratory ambient disturbances and within 9 nanometers RMS under severe forced resonant disturbances.

2. Introduction

The next generation of space based astronomical missions will require long baseline optical interferometry for higher angular resolution and sensitivity. Figure 1 shows one possible configuration in which any two of the six star light collector telescopes form a long baseline interferometer. The astrometric accuracy of the interferometer improves with longer baseline. For the instrument to perform its mission successfully, the variations in the length of the paths traveled by star light through the pair of collectors to the detector must be no more than 15 nanometers RMS [1]. An additional requirement is to maintain the wave front tilt of the collected star light within a few micro-radians RMS [1]. The complexity of

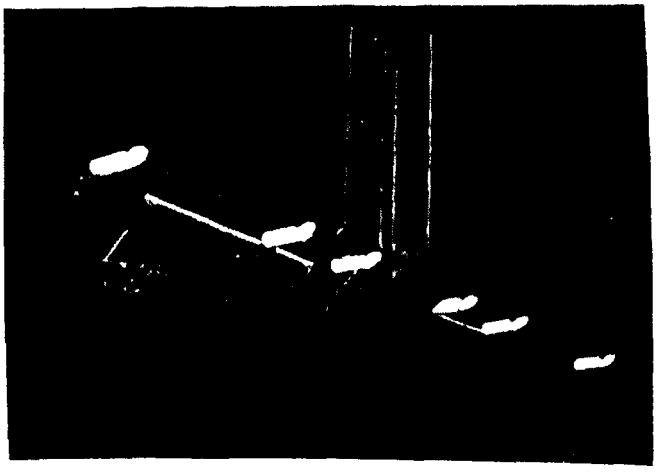

achieving and maintaining these stringent requirements increases as collectors are mounted on large flexible structures, Also a longer baseline usually implies a more flexible base structure that results in a more severe interaction of the base dynamics with the control system. As a result, Control Structure interaction (CSI) becomes an important issue in designing the compensation system for optical pathlength control.

In this paper, we present results of structural control and optical pathlength control experiments with an optical setup which couples non-collocated structural motions in the optical path. The target mirror and the actuators are placed in a non-collocated fashion and the traveling Light is allowed to bounce off two flexible booms on the JPL precision truss structure (Figure 2). In this setup, optical control alone is not sufficient to achieve the required performance level of pathlength variation since lightly damped non-collocated structural modes at low frequencies are present within the desired controller

* Member Technical Staff, Applied Mechanics Section
† Member Technical Staff, Guidance and Control Section

bandwidth . The damping of selected structural modes "is enhanced by implementing a structural control layer which enables a high bandwidth optical controller for direct pathlength compensation. The optical controller maintains pathlength variations within 6 nanometers RMS when only the laboratory ambient disturbance is present and within 9 nanometers RMS when a forced disturbance is induced at a dominant resonant frequency.

In earlier experiments performed by O'Neal and Spanos[2], optical pathlength was effectively controlled to 3 nanometers RMS. The experiments used an optical configuration that isolated structural motion from the optical path. The target mirror in the configuration was placed on a rigid frame which was unrealistic for an actual space mission. In separate experiments by the authors [3,4], the target mirror was placed on a flexible truss structure along with the compensation system. They observed a large coupling of structural motion to optical pathlength and were able to control the variations down to 5 nanometers RMS. In this setup, the target mirror and the actuators were placed in such a way that it effectively formed a collocated sensor-actuator system. All the structural modes were interacting stably with a phase lead controller as expected. However few localized modes at higher frequencies caused loss of the collocation which limited the bandwidth of the control loops.

3. JPL Phase B Testbed

To address the control structure interaction (CSI) issue associated with the long baseline interferometer, JPL (Jet Propulsion Laboratory) has developed a ground test bed facility known as the JPL Phase B testbed (Figure 2). A detailed description of the test bed is available in reference [5], The testbed is an eight foot tall precision truss structure cantilevered at the base and has two horizontal truss booms (called X and Y booms) at the top,

The optical element attached to the X boom of the testbed represents a optical delay Line for a stellar interferometer telescope. The optical delay line for optical pathlength compensation system with laser light trace to simulate star light is shown in Figure 2. The delay line is equipped with a primary parabolic mirror and a secondary plane mirror placed at the focal point of the primary mirror. The mirror setup is rigidly encased in an invar trolley suspended from the structure with soft flexures. The secondary mir-

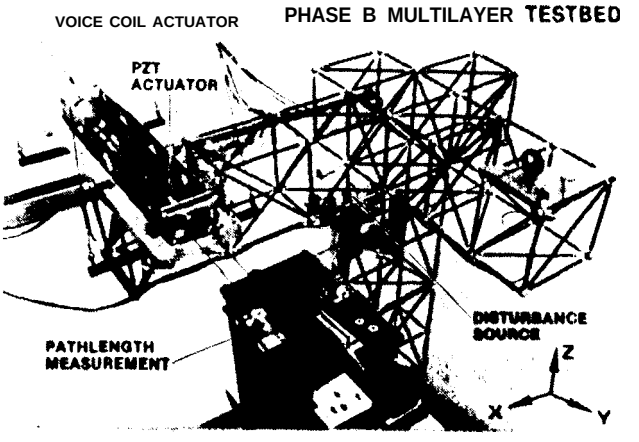

Figure 2: JPL Phase B Testbed with optical delay-line and option 2 optics (Laser light simulates starlight).

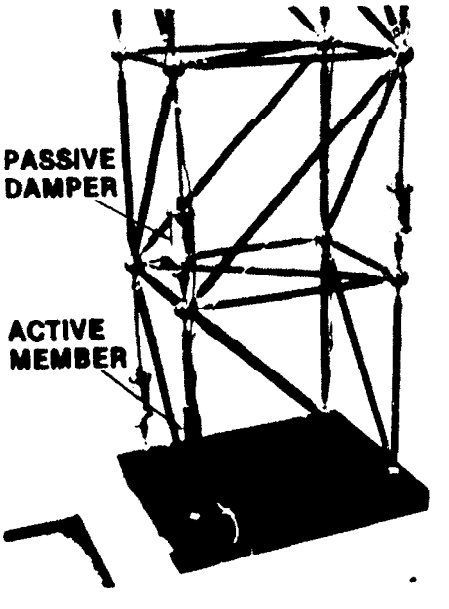

Figure 3: Active and passive dampers embedded into JPL Phase B Testbed

ror is driven relative to the trolley by a reaction compensated PZT (piezoelectric) actuator for fine pathlength adjustment. The trolley is driven by a voice coil actuator for coarse pathlength compensation. The optical behavior of the setup is more like a retroreflector with a capability of providing coarse (millimeter) to very fine (nanometer) pathlength compensation over a wide frequency bandwidth. Since the delay line compensation system and the target retroreflector are installed on different truss booms (Figure 2), the motion of the boom with the retroreflector causes the loss of actuator-sensor collocation.

in the pathlength compensation system, Retroreflector and Plane Mirror Interferornetry are combined such that the optical alignment is maintained under translational and rotational motions. This optical configuration, as compared to retroreflector interferometry or plane mirror interferometry, is less likely to 1osc its alignment due to the structural vibration. The laser beam passes eight times through the trolley, as compared to two times in retroreflector interferometry or four times in plane mirror interferometry, resulting in an enhanced laser metric resolution.

4.0 Structural Control

Due to the lightly damped truss structure and the non-collocation of the optical setup, design of a robust high bandwidth and high authority optical pathlength compensator is extremely difficult without enhancing structural damping. The frequency response functions (FRF) of voice coil actuator to laser pathlength variation is shown in Figure 4. The FRF with no structural control, represented by the dashed line, contains a large number of lightly damped modes and some of which are non-collocated. It turns out that a low bandwidth and moderate gain voice coil compensator that can be designed with reasonable stability margins is not adequate to achieve the performance level that is required to keep optical pathlength variations below 15 nanometers RMS.

Four passive Honeywell viscous dampers [6] and four active members [7,8] are deployed (Figure 3) to enhance modal damping and thereby make the structure quiet. The locations of the active and passive members are chosen to maximize the energy dissipation of a specific set of modes using the simulated annealing strategy [9]. The stiffness and the damping coefficient of the passive dampers can not

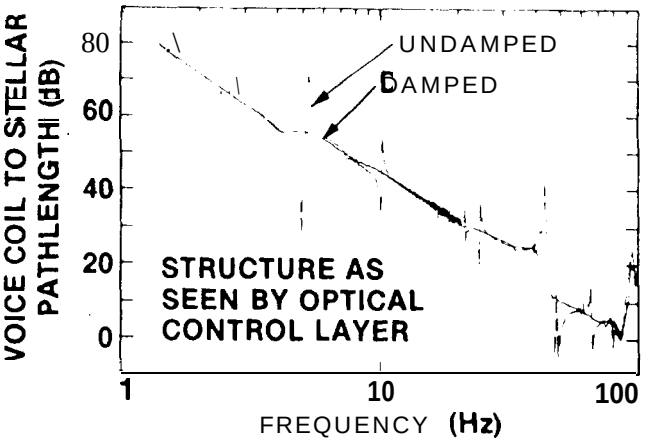

Figure 4: Voice coil to optical pathlength frequency response function before and after structural control

be altered. By contrast, these parameters for the active members can be tuned through simple collocated bridge feedback control [4,10,1 1] or force feedback control [12,13] to achieve optimal damping performance. To facilitate this, a load cell to measure the force exerted at the interface of the active member and the remainder of the structure and an eddy current sensor to measure the extension of the member are present in each active member. The actuator part of these active members is prestressed high voltage piezoelectric stacks and is driven by high voltage power amplifiers, Because of their tunability, the active members are used to enhance damping of selected higher frequency structural modes. The FRF of voice coil to the laser pathlength for the damped structure (Figure 4) and the disturbance transmission function (Figure 5) from a disturbance shaker input to the laser pathlength show a significant enhancement of damping for structural modes up to 100 Hz. The damping in the major modes has been increased from fractions of a percent of critical to more than 5%.

4.1 Impedance Matching for structural damping

The impedance of a mechanical element is defined by the ratio of extension rate (relative velocity) of the element to force that caused the extension. For example, a linear spring with stiffness K has impedance $\frac{s}{K}$, where s is the Laplace variable. Spring impedance is a positive imaginary quantity over the entire frequency range indicating that springs are energy conserving elements. A linear viscous damper with damping coefficient C has impedance $\frac{1}{C}$ which is a positive real quantity over the entire frequency range indicating that dampers

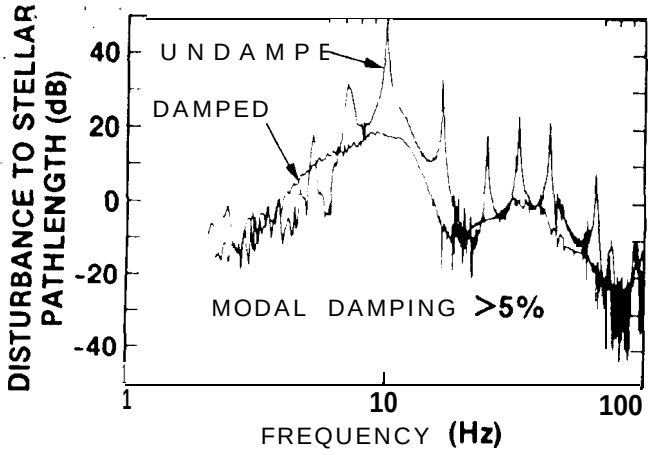

Figure .5: Disturbance attenuation by Structural Control

arc purely energy dissipative elements.

The concept behind matching the impedance of an active member to that of the structure is based on increasing damping for maximum vibrational power dissipation. It is shown that in order to effect maximum rate of energy dissipation through the active member, the impedance of the active member should be made equal to the complex conjugate of the structure's impedance at the interface point. Meeting the impedance matching condition exactly on flexible structures is not practical because lightly damped structures contain sharp resonances in their impedance functions that are highly sensitive to perturbations in structural parameters such as natural frequency. In addition, the complex conjugate of the impedance of a structure is a non positive-real function that cannot be approximated over a broad frequency range with stable electrical circuits. Alternatively, if the active member's impedance is made equal (matched) to the smoothed average impedance [4,10] of the structure over the frequency range of interest, an excellent damping performance is achieved.

Figure 6a and 6b describe a complete force feedback control system for enhancing modal damping by matching the impedance of an embedded active member to that of the structure. The area enclosed by the dashed line represents an active member (without the feedback) embedded in the structure where *V(s), X(s)* and $F(s)$ are respectively the active member driver voltage, the member relative extension and the interface force between the member and the structure. $Z_0(s)$ is the open loop ac-

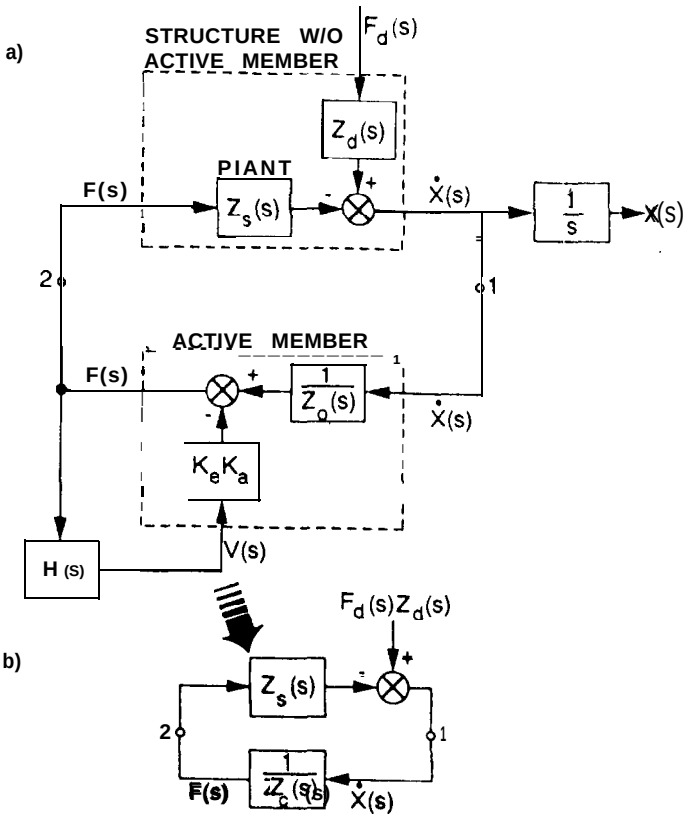

Figure 6: Active darnping via Force Feedback

tive member impedance when voltage is held to a constant bias value. It is essentially a spring with stiffness K_a and impedance

$$Z_0(s) = \frac{s}{K_a} \tag{1}$$

where K_a is equal to the sum of the stiffnesses of the piezoelectric stack and the preload spring in the member (preload spring is normally much softer than the stack), The piezo-motor constant, K_e, is the ratio of extension $X(s)$ to applied voltage $V(s)$ when force $F(s)$ is held to zero. This constant is equal to the product of the piezoelectric voltage coefficient of the material, the length of piezoelectric stack, the voltage amplifier gain and the ratio of the stack stiffness to K_a. Obviously the value of K_e should be experimentally determined before installation to enforce the condition of $F(s) = O$. 'I'he plant, defined to be the structure without the active member with input and output being respectively the force and the relative extension rate at the interface point with the active member, is represented by the block containing $Z_s(s)$. Where $Z_s(s)$ is the impedance of the plant (ie. the structure without the active member) and is measured at the interface

point of the structure and the active member. It is a function of the structural property of the structure and it contains all the modes that are controllable/observable from the interface point. $F_d(s)$ is a disturbance force input to the structure. The structural impedance $Z_d(s)$ is measured from the disturbance input point to the relative extension rate output point (at the interface of the structure and the active member) when the active member is physically removed. $Z_d(s)$ may or may not contain all modes whose damping are being enhanced and its explicit determination is not necessary. The feedback loop is closed through the compensator block $H(s)$ and the loop transmission from point 1 to point 2 is the inverse of impedance $Z_c(s)$ that appears of the active member from the interface point and is depicted in Figure 6b. Here $Z_c(s)$ is the active member impedance when the feedback loop is closed through the block H (s), and the active member impedance is $Z_0(s)$ when the loop is open. It is important to note that $Z_c(s)$ and 2.(s) are the properties of the active member without the structure and likewise $Z_s(s)$ and $Z_d(s)$ are the properties of the structure without the active member.

Active member's extension rate is related to applied voltage, active member open loop impedance and interface force at boundary by the following relation

$$\text{i(s)} = V(s)K_e s + F(s)Z_0(s) \qquad (2)$$

$$\text{or, } F(s) = \frac{1}{Z_0(s)}\text{i(s)} - K_a K_e V(s) \qquad (3)$$

The extension rate expression is a superposition of two components: the first component is due to applied voltage $V(s)$ and the latter one is due to the presence of interface force $F(s)$. Equation 3 that characterizes the active member is represented inside the box labelled 'Active Member' in Figure 6a.

Relative extension rate of the structure at the interface with the active member due to disturbance force 1:(s) is given by the following relation

$$\text{i(s)} = Z_d(s)F_d(s) - Z_s(s)F(s) \qquad (4)$$

The first component of Equation 4 is the extension rate that the structure would exhibit at the interface point if no active member is present (ie. 1'(s) = O) and the second one incorporates the effect of non zero interface force due to the presence of the active member. The interface force $F(s)$ develops due to the fact that the structure is interfaced with an active member with impedance $Z_c(s)$ (or $Z_0(s)$ when the feedback loop is open) and the structure is disturbed by the disturbance force $F_d(s)$ (see Fig. 6a). The negative sign in the equation is necessary to satisfy the compatibility condition while the impedances are consistent with the earlier definition.

Let $\dot{X}(s)$ and $F(s)$ be the closed loop extension rate and force respectively due to the disturbance force $F_d(s)$, then the closed loop active member must satisfy the following condition

$$Z_c(s) = \frac{\dot{X}(s)}{F(s)} \qquad (5)$$

$$\text{or, } F(s) = \frac{\dot{X}}{Z_c(s)} \qquad (6)$$

solution of Equations 4 and 6 yield the relative extension rate and the interface force as explicit functions of the structural and active member impedances and the disturbance force as shown below

$$\dot{X}(s) = \frac{Z_c(s)}{[Z_c(s) + Z_s(s)]} Z_d(s)F_d(s) \qquad (7)$$

$$F(s) = \left[\frac{1}{Z_c(s) + Z_s(s)}\right] Z_d(s)F_d(s) \qquad (8)$$

We assume that the disturbance force $f_d(t$ (Laplace transform of $f_d(t)$ is equal to $F_d(s)$) can be represented by the following finite series

$$f_d(t) = \sum_{k=1}^{N} A_k e^{j\omega_k t} + \text{c.c.} \qquad (9)$$

where cc. and j represent the complex conjugate part and $\sqrt{-1}$ respectively. Equation 7, 8 and 9 may be used to derive an expression for the steady state active member power dissipation $P(t)$ which is the product of the steady state extension rate, $\dot{x}_{ss}(t)$, and the steady state interface force, $f_{ss}(t)$,

$$P(t) = \dot{x}_{ss}(t) \cdot f_{ss}(t)$$

$$\text{or, } = \left(\sum_{k=1}^{\text{lv}} \frac{Z_c(j\omega_k)}{Z_c(j\omega_k) + Z_s(j\omega_k)} Z_d(j\omega_k)A_k e^{j\omega_k t} + \text{Cc.} \sum_{(n=1}^{N} \frac{1}{Z_c(j\omega_n) + Z_s(j\omega_n)} \cdot Z_d(j\omega_n)A_n e^{j\omega_n t} + \text{c.c.}\right) \qquad (10)$$

When expanded, the product on the right hand side of the Equation 10 contains time varying and non-time varying components, The time varying component which is oscillatory represents the conservative parts of the power ie. equal amount of energy is

withdrawn from arid then put back into the structure by the active member. As a result, it does not contribute to net energy dissipation. On the other hand the non-time varying parts being positive real (a constraint on $Z_c(s)$ is imposed later) represent the purely dissipative part of the power, P_{diss} and is given by

$$P_{diss} = \sum_{k=1}^{N} \frac{Z_c(-j\omega_k)}{Z_c(-j\omega_k) + Z_s(-j\omega_k)} \cdot \frac{1}{Z_c(j\omega_k) + Z_s(j\omega_k)} |Z_d(j\omega_k) A_k|^2 + \text{Cc.} \quad (11)$$

Since we intend to modify $Z_c(s)$ to effect maximum power dissipation, the variation of P_{diss} with respect to $Z_c(j\omega_k)$ for all $k = 1,2,\ldots N$ must vanish ie.

$$\delta P_{diss} = 0 \quad (12)$$

As $Z_c(j\omega_k)$ and in-turn $\delta Z_c(j\omega_k)$ for all $k = 1,2,\ldots N$ are independent, Equation 12 reduces to

$$\frac{\partial P_{diss}}{\partial \text{Re}[Z_c(j\omega_k)]} = 0 \quad (13)$$

$$\frac{\partial P_{diss}}{\partial \text{Im}[Z_c(j\omega_k)]} = 0 \quad (14)$$

for all $k = 1,2,\ldots N$. Substitution of Equation 11 into Equation 13 and 14 and the subsequent solution yield

$$\text{Re}[Z_c(j\omega_k))] = \pm \text{Re}[Z_s(j\omega_k))] \quad (15)$$

$$\text{Im}[Z_c(j\omega_k))] = -\text{Im}[Z_s(j\omega_k))] \quad (16)$$

for all $k = 1,2,\ldots N$. The stipulation that the power be dissipative requires that the expression with positive sign in Equation 15 be chosen which leads to

$$\text{Re}[Z_c(j\omega_k)] = \text{Re}[Z_s(j\omega_k)] \quad (17)$$

for all $k = 1, 2, \ldots, N$. Equation 16 and 17 establish the fact that the active member impedance be equal to the complex conjugate of the structure's at frequencies where maximum-energy dissipation rate is desired. When multiple active members are present in the structure Equation 11 should be modified to include the effect of all active members before the necessary condition (Equation 12) is imposed,

4.2 Force Feedback for Impedance Matching

In Force Feedback of structural control, the controller $H(s)$ is usually a pure integrator with a constant gain K_I

$$H(s) = \frac{K_I}{s} \quad (18)$$

Hence, tile input voltage to the active member has the following form

$$v(s) = F(s)\frac{K_I}{s} \quad (19)$$

Substitution of Equation 19 into Equation 2 yields

$$i(s) = F(s)\frac{K_I K_e}{s} s + F(s) Z_0(s) = F(s)[K_e K_I + Z_0(s)] \quad (20)$$

$$Z_c(s) \equiv \frac{i(s)}{F(s)} = K_I K_e + Z_0(s) \quad (21)$$

Equation 1 is substituted into the equation above which yields

$$Z_c(s) = K_I K_e + \frac{s}{K_a} \quad (22)$$

Equation 22 shows that the closed loop active member, as it appears to the structure, is equivalent to a series combination (Figure 7) of a damper and a spring with damping coefficient of $\frac{1}{K_e K_I}$ and spring stiffness of K_a respectively. The problem with this configuration is that it possesses no static stiffness and will accommodate undesirable permanent deformation. Also implementation of a pure integrator is practically impossible as presence of nonzero bias/drift of the force measuring load cell will cause saturation of the integrator and the active member. However, the stiffness of the member at and near DC can easily be improved by adding a 1st order high pass filter to the compensator, In our experiment a high pass filter with corner frequency at 1 Hz (ω_0 = 6.28 rads/see) is provided for the load cell of each active member. The resulting H(s) is a 1st order low pass filter with a pole at $-\omega_0$

$$H(s) = \frac{K_I}{s} \cdot \frac{s}{s + \omega_0} = \frac{K_I}{s + \omega_0} \quad (23)$$

The closed loop active member behavior is modified to an elastically coupled damper as depicted in Figure 8 and its impedance is given by

$$Z_c(s) = \frac{1}{\frac{1}{K_e K_I} + \frac{\omega_0}{K_e K_I s}} + \frac{s}{K_a} \quad (24)$$

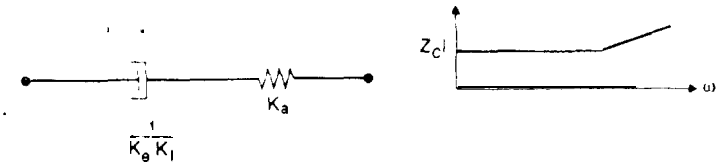

Figure 7: Active member closed loop impedance

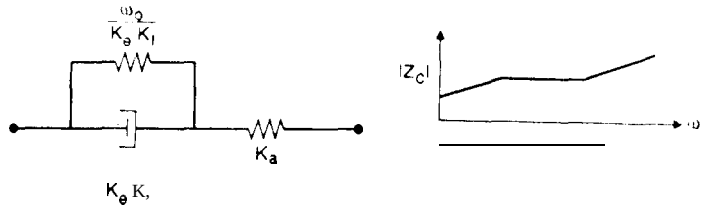

Figure 8: Active member closed loop impedance with high pass filter

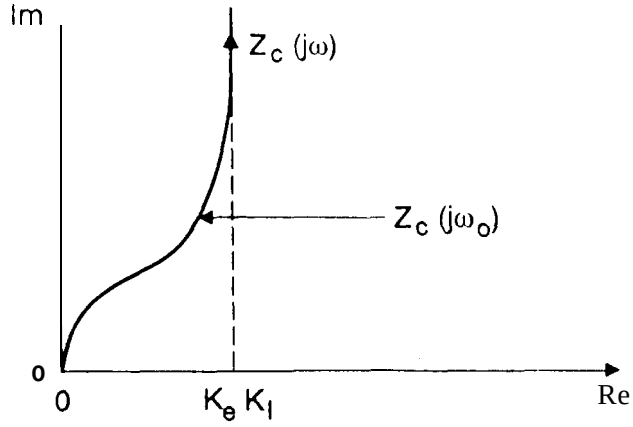

Figure 9: Plot of $Z_c(j\omega), \omega > 0$

The stiffness of the spring parallel to the damper is $\frac{\omega_0}{K_e K_I}$. This modification is necessary to recover the static shape of the structure under no-load condition and to avoid saturation of the integrator and the active member. Finally, an approximate impedance match is obtained by adjusting the value of K_I. Also, one has the option of modifying the value of ω_0 to improve the match.

The question arises of how the presence of one or multiple closed loop active members in a structure affects stability. Due to the fact that a closed loop active member appears to the structure as $Z_c(s)$ which emulates a (elastically coupled) passive damper since $\mathrm{Re}[Z_c(j\omega)] > 0$ for w > 0 as shown in Figure 9 (recall that a damper has positive real impedance), presence of one or multiple active members in a structure increase structural damping and do not cause instability in the structure. Coupled with this is the fact that the sensor and actuator of the active member are collocated, and therefore the stability of the system is robust.

The structural impedance $Z_s(s)$ is determined by exciting the structure with the active member, and measuring (the negative of) the ratio of the velocity across the active member to the force exerted at the interface. The impedance 2.(s) of the active member without feedback is obtained by exciting the structure with a shaker attached to the structure, and measuring the ratio of velocity to the force at the interface,

No effort has been made to optimize the impedances of the four active members simultaneously. The impedances are optimized in a successive manner ie. one after another. However with this suboptimal approach, we have achieved an excellent damping performance.

5. Optical Control

The optical control (or optical delay line control) for direct optical pathlength compensation is designed to provide coarse (millimeter) to very fine (nanometer) pathlength compensation over a wide frequency bandwidth. The coarse and fine compensations are provided respectively by the voice coil and the PZT actuators in the delay line. The delay line is described in more detail in section 3.

The architecture of this two input (voice coil and PZT) and one output (pathlength) control system is shown in figure 10, Use of a similar architecture in pathlength control experiments has been reported in references [2-4,14]. $G_1(s)$ and $G_2(s)$ are the transfer functions respectively from PZT and voice coil to pathlength, and $K_1(s)$ and $K_2(s)$ are the compensators respectively for the PZT and the voice coil actuators. Note that the output of the PZT controller ($K_1(s)$) drives both the PZT actuator and the voice coil controller ($K_2(s)$). The open loop transfer function for the system with the given architecture is

$$L = K_1(G_1 + K_2G_2) \tag{25}$$

'I'he objective is to design the two compensators $K_1(s)$ and $K_2(s)$ such that the closed loop system is stable with adequate gain and phase margins, and the total loop gain $|L(j\omega)|$ is large over the largest achievable bandwidth since the disturbance rejection

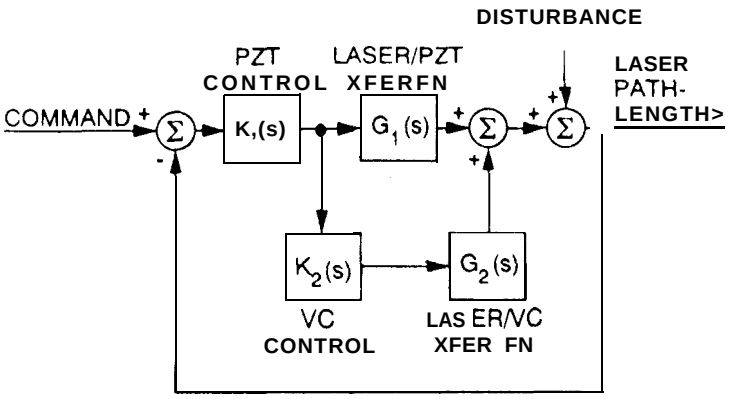

Figure 10: Control system Architecture

is proportional to $|L|$ when $|L|$ is large. The following properties are observed from Equation 25:

$$I, \approx K_1 K_2 G_2 \text{ when } |K_2 G_2| \gg |G_1| \quad (26$$

$$L \approx K_1 G_1 \text{ when } |K_2 G_2| \ll |G_1| \quad (27$$

At low frequency where the voice coil loop gain is large, the total loop gain is equal to the product of the voice coil loop and the PZT compensator gains. At high frequency, the total loop gain approaches the PZT loop gain as the voice coil loop gain approaches zero. As a result, at low frequencies where the pathlength variation is normally large, the voice coil forward loop $(K_2(s)G_2(s))$ being dominant prevents the limited stroke length PZT actuator from saturation. At high frequencies where the pathlength variation is smaller, the PZT forward loop $(K_1(s)G_1(s))$ is dominant and relieves the limited frequency bandwidth voice coil.

Bode's classical control design methods [15] are used to design compensators $K_1(s)$ and $K_2(s)$ to shape the open loop system in the frequency domain. This design methodology does not require an explicit parametric model of the plant but rather uses the measured frequency response functions to synthesize the compensators, The two controllers having authorities at two different frequency ranges are blended smoothly along the whole frequency range of interest.

Controllers are designed one loop at a time. The voice coil controller is designed to stabilize the system assuming that it is driven by the pathlength measurement and the the PZT actuator is disconnected. The controller is an 8th order filter including a 2nd order lead filter to provide adequate phase

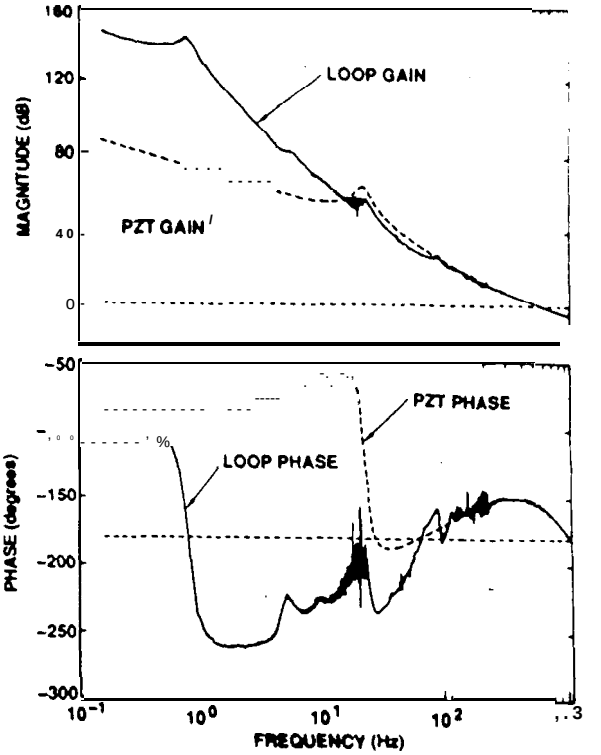

Figure 11: Bode plot of optical control

margin at the cross-over frequency (approximately, 35 Hz) followed by seven 2nd order notch filters (-3 dB) to provide additional gain margin over 7 local modes at the high frequencies.

The controller for the PZT consists of a first order lag filter and a second order low pass filter. The lag filter provides a high gain at low frequency for good disturbance rejection and the low-pass filter provides at high frequency a -20 dB/Dec steep gain roll off with an adequate phase margin for stable control structure interactions, The PZT control loop bandwidth is limited to approximately 500 Hz due to high frequency noise and digital implementation delay, The Bode plot of the optical control loop gain is shown in figure 11,

Both control laws are discretized using pole-zero mapping with zero padding. The effects of time delays due to the computer implementation and the zero order hold are incorporated in determining the actual phase margin, The low bandwidth voice coil controller and the, high bandwidth PZT controller are implemented at 2,000 Hz and 10,000 Hz respectively,

6. Experiment

The PZT controller K_1 and the voice coil controller K_2 are implemented respectively in V3E/50MHz and V3E/20MHz single board computers (SBC) with a VME bus interface. A third V30/25MHz single board computer is employed to synchronize the control activity and store the time data for later analysis. All programs are written in C language and utilize VxWorks routines for timing the control loops.

A Tektronix *2630* network analyzer is used to derive all the frequency response functions (FRF). A combination of band limited white noise and sine swept inputs are used to generate the FRFs with high coherence levels. The PZT actuator to the pathlength FRF is fairly unaffected by the flexibility of the structure because the mass of the primary mirror on the PZT actuator is small and the PZT actuator is reaction compensated. The compensation is achieved by installing another PZT actuator reacting equally in the opposite direction of the control PZT actuator, The phase of the FRF has a negative slope equivalent to -70 μs pure time delay, while the magnitude is relatively constant. This delay is found mainly due to the time needed to transfer of data from the laser metric system to the analyzer.

The voice coil to the pathlength FRF (Figure 4) without structural control is significantly affected by the structural flexibility. The dominant peak at 0.7 Hz (not shown in the figure) is due to the flexure that attaches the trolley to the truss. All other peaks in the FRF correspond to structural modes of the truss. At 80 Hz the phase drops rapidly while modal density and plant uncertainty increases considerably. This leads us to limit the voice coil loop bandwidth to a frequency lower than 80 Hz. The non-collated modes severely limits the bandwidth of the voice coil controller which, along with the PZT controller, is unable to maintain the pathlength within the prescribed variation. As mentioned before 4 passive and 4 active dampers are deployed to damp out these modes and the final voice coil controller with large bandwidth and adequate stability margin is designed.

The first experiment is carried out to determine the disturbance transmission from a disturbance shaker attached at the mid bay area of the truss. The dashed line in Figure 12 illustrates the disturbance transmission function from the shaker to pathlength

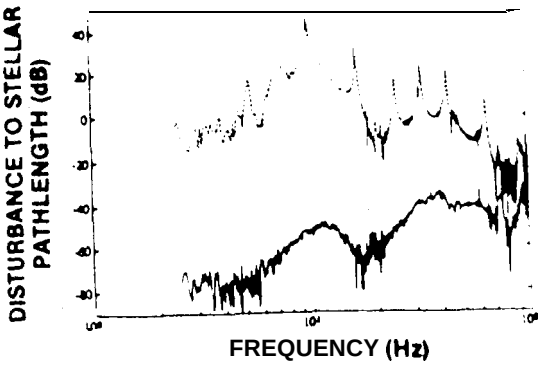

Figure 12: Disturbance attenuation due to structural and optical control

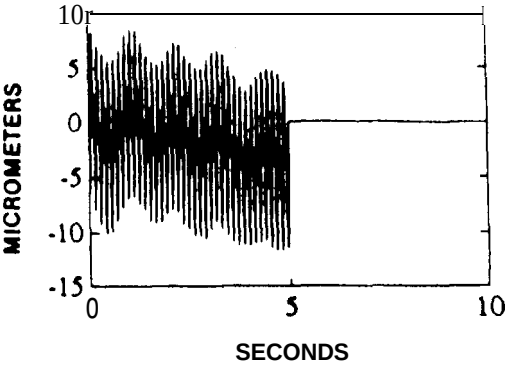

Figure 13: Optical pathlength variation due to resonant excitation (7.3 Hz)

when no structural control (no damping enhancement) and no optical control are present. One can easily see the very lightly damped structural resonances in the pathlength output. The solid line in the figure is the transmission function when both structural and optical controls are deployed. The disturbance rejection is very dramatic ranging from -80dB at the low frequencies to -30 dB at 100 Hz. The bandwidth of the controller is experimentally determined to be approximately 500 Hz.

Two additional closed loop experiments are carried out - the first one demonstrates rejection of the ambient laboratory disturbances and the second one demonstrates rejection of a forced resonant disturbance (at 7,3 Hz) induced by the disturbance shaker, In both experiments, after recording open loop pathlength histories for five seconds the control loops are closed and the closed loop pathlength histories are recorded for an additional five seconds. The open loop pathlength variation due to the laboratory ambient disturbance has been reduced to 6 nanometer

RMS from 1.3 micrometer RMS a disturbance rejection of -47dB. A spectral analysis of the open and closed loop data indicates that the achieved bandwidth is approximately 450 Hz and a large part of the closed loop pathlength error is due to the noise at frequencies beyond the controller bandwidth. Figure 13 illustrates the resonant response experiment. The first five seconds of the response are dominated by the 7.3 Hz resonant disturbance input to the structure. The closed loop response is down to 8.5 nanometers from 5.6 micrometers - a rejection of -57 dB.

7. Conclusion

We have successfully designed and implemented structural and optical pathlength control systems for flexible testbed structures to be used for future space missions in optical interferometry. The two layer control (structural control and optical control) designs have been carried out in the classical frequency domain by directly shaping the measured input/output response functions. The structural control which enhances structural damping has enabled the high bandwidth optical pathlength control for improved performance. The impedance matching technique has been used successfully to increase the modal clamping in an optimal fashion. In optical control, to increase the compensation range over a large bandwidth, a smooth blending of the two controllers (large stroke and small stroke) having authorities at two different frequency ranges has been implemented, Experiments have been carried out to determine the disturbance transmission function and the effective rejection of the laboratory ambient and shaker induced disturbances. The results so far supports that nanometer level optical pathlength control is feasible in space. It should be mentioned that the optical wave front tilt control has not been addressed yet and is now a topic of research at J P L.

8. Acknowledgments

This research has been performed at the Jet Propulsion Laboratory of the California Institute of Technology under a contract with the National Aeronautics and Space Administration sponsored by the Office of Aeronautics and Space Technology, Code RM. The authors also acknowledge the help of Mike Kantner in designing the post filters and the cooperation of the whole CSI group in completing the experiment,

9. References

1. Laskin, R.A. and San Martin, A.. "Control/Structure System Design of a Space borne Optical Interferometer," AAS/AIAA Astrodynamics Specialist Conference, 1989.

2. O'Neal, M.C. and Spanos, J,'l'., "Optical pathlength Control in the Nanometer Regime on the JPL Phase B Interferometer Testbed," SPIE International Symposium on Optical Applied Science and Engineering, 1991.

3. Spanos, J.T. and Rahman, Z., "Optical Pathlength Control on the JPL Phase B Interferometer Testbed," 5th NASA/DoD CSI '1'ethnology Conference, 1992.

4. Rahman, Z., Spanos, J. and Fanson, J., " Experiments on Active Optical and Structural Control," Proceedings of 31st IEEE Conference on Decision and Control, pp. 1824-1829, 1992.

5. Eldred, D.B. and O'Neal, M. C., "The JPL Phase B Test bed Facility," A DPA Active Materials and Adaptive Structures Symposium and Exhibition, 1991.

6. Wilson, J.F. and Davis, L. P., "Viscous Damped Space Structure for Reduced Jitter," 58th Shock and Vibration Symposium, 1987.

7. Anderson, E. H., Moore, D. M., Fanson, J, L. and Ealey, M. A., "Development of an Active Member Using Piezoelectric and Electrostrictive Actuation for Control of Precision Structures," 31st AIAA Conference on Structures. Structural Dynamics and Materials, 1990, paper no, AIAA-9O-1O85-CP.

8. Anderson, E. H., Moore, D, M., Fanson, J .L. and Ealey, M. A., "Development of an Active Truss Element for Control of Precision Structures," Optical Engineering, vol. 29, no. 11, pp. 1333-1341, 1990.

9. Chu, C. C., Fanson J.I,., Milman, M.H. and Eldred, D, B., "Optimal Active Member and Passive Member Placement and Tuning," 4th NASA/DoD Control/Structures Interaction Tech Conference, 1990.

10. Chen, G-S., and Lurie, B., "Bridge Feedback for Active Damping Augmentation," AIAA Journal of Guidance and Control, To appear.

11. Fanson, J.L., Chu, C.C. and Lurie, B. J., "Damping and Structural Control of JPL l'base O Testbed Structure," First Joint U.S./Japan Conference on Adaptive Structures, 1990.

12. Rahman, Z., Spanos, J., O'Brien, J., and Chu, C- C., "optical Pathlength Control Experiment on J PL l'base B Test bed," 34th AIAA Conference on Structures, Structural Dynamics and Materials, 1993, paper no. AIAA-93-1695-CP.

13. O'Brien, J., "Discussion and Experimental Results of Integral Force Feedback for Structural Damping," Inter-office memorandum no. 354:92:019:JOB, JPL, 1992,

14. Colavita, M. M., "Prototype High Speed Optical Delay Line for Stellar Interferometry," SPIE International Symposium on Optical Applied Science and Engineering, 199].

15. Bode, H. W., Network Analysis and Feedback Amplifier Design, Van Nostrand, NY, 1945,